Algal Research 86 (2025) 103917

Contents lists available at ScienceDirect

Algal Research

journal homepage: www.elsevier.com/locate/algal

Parameter estimation in anoxic aerobic algal-bacterial photobioreactor devoted to carbon and nutrient removal

Irina Bausa-Ortiz [a,b,*], Raúl Muñoz [b,c], Andrés F. Torres-Franco [b,c], Smaranda P. Cristea [a,b], Cesar de Prada [a,b]

[a] Department of Systems Engineering and Automatic Control, University of Valladolid, Paseo Prado de la Magdalena 3-5, Valladolid 47011, Spain
[b] Institute of Sustainable Processes, Paseo Prado de la Magdalena 3-5, Valladolid 47011, Spain
[c] Department of Chemical Engineering and Environmental Technology, University of Valladolid, Real de Burgos s/n, Valladolid 47011, Spain

ARTICLE INFO

Keywords:
Microalgae-bacteria consortia
Modeling
Optimization
Simulation
Wastewater treatment

ABSTRACT

The increasing number of microalgae-based applications demands the development of model-based information and decision support systems that can deal with their complex behavior, particularly the interactions in mixed algal-bacterial wastewater treatment systems. This work aimed to estimate the parameters for modeling and simulating an anoxic-aerobic algal-bacterial photobioreactor with biomass recycling for treating high-strength wastewater. Estimating the model parameters was critical in applying the model to anoxic-aerobic algal-bacterial systems. Process model and simulation were developed using the dynamic simulation software PROOSIS®. The model was set up and then calibrated with data from a lab-scale plant treating different dilutions of digestate. Simulations and model performance metrics validated the capability of the calibrated mathematical model to predict the experimental results.

1. Introduction

The use of microalgae has become a promising technology for wastewater treatment as it helps to reduce the high energy costs associated with mechanical aeration in conventional wastewater treatment [1]. Domestic and industrial wastewaters and anaerobic digestion effluents are characterized by high carbon, nitrogen, and phosphorus loads that must be treated before discharge into natural water bodies to avoid oxygen depletion, toxicity issues, and eutrophication. In this context, the capacity of microalgae to simultaneously remove carbon, nitrogen, and phosphorus via mixotrophic assimilation represents an essential advantage in comparison with aerobic activated sludge or anaerobic digestion technologies in terms of enhanced nutrient recovery. Therefore, the further use of the harvested microalgae biomass to produce biofertilizers, biofuels, and other bioproducts makes this technology an attractive alternative for cost-effectively combining wastewater treatment and nutrient management [2,3].

Microalgae are photosynthetic microorganisms that grow using inorganic carbon as a carbon source and light as an energy source. Despite of their many advantages, these technologies may present certain limitations related to their industrial exploitation, such as the selection of the optimum strains and cultivation parameters, including temperature (which vary between 20 and 40 °C, depending on the strains [4,5]), pH, light intensity, reactor type, and nutrient concentration in wastewater. Indeed, numerous experimental studies have been conducted to determine the influence of these cultivation parameters on nutrient removal efficiency and biomass productivity for different microalgae strains and operational conditions [6–12]. Similarly, several research works have focused on maximizing nutrient removal in high-rate algal ponds (HRAPs) and other photobioreactor configurations [13–15]. Besides the experimental approach, recent developments and improvements in mathematical modeling, simulation, instrumentation, and process control can contribute to selecting the optimal conditions for microalgae cultivation, whether for high-value product production or nutrient removal.

Mathematical modeling, a key tool for designing, analyzing, and operating chemical processes, has been successfully applied in the field of microalgae research. Despite the challenges of bioprocesses modeling, there are successful precedents, such as the application of mathematical models like the Activated Sludge Models (ASM) [16] in wastewater

* Corresponding author at: Department of Systems Engineering and Automatic Control, University of Valladolid, Paseo Prado de la Magdalena 3-5, Valladolid 47011, Spain.
E-mail address: irina.bausa@uva.es (I. Bausa-Ortiz).

https://doi.org/10.1016/j.algal.2025.103917
Received 25 June 2024; Received in revised form 20 November 2024; Accepted 11 January 2025
Available online 17 January 2025

treatment. The River Water Quality Model 1 (RWQM1) [17], developed by the International Water Association (IWA) Task Group on River Water Quality Modeling represented a milestone in the modeling of microalgae and bacteria interactions. Since the formulation of RWQM1, other mechanistic models have been proposed to simulate microalgae-based wastewater treatment plants. These models have been rigorously tested and successfully validated in various photobioreactor configurations operating under different operational conditions [18–22], reassuring the research's reliability in this field.

Nowadays, research is also focused on the design and improvement of facilities for optimizing microalgae biomass yield and improving nutrient removal from wastewater. In this regard, anoxic-aerobic microalgal-bacterial systems have emerged as a highly efficient alternative for removing nutrients from wastewater with low carbon to nutrient radio [23–26]. Among these systems, a novel anoxic-aerobic configuration has shown promising results in the treatment of digestates [27]. This kind of configuration is still in the research stage before being implemented on a larger scale. As part of the test stage, this novel photobioreactor configuration demands several experiments to evaluate their performance and nutrient removal efficiencies under various operational conditions and to treat different types of wastewater. This evaluation is of utmost importance, as it provides crucial insights into the effectiveness of the anoxic-aerobic photobioreactor configuration. However, these experiments are highly time-consuming and resource-consuming. Mathematical modeling applied to this novelty system is a helpful tool for predicting and understanding the processes occurring in each plant element, allowing the simulation of a broad range of experimental and operational conditions in a few minutes. Unfortunately, the mathematical modeling of this promising anoxic-aerobic algal-bacterial configuration has not been conducted to date.

This work aims at modeling and simulating dynamically an anoxic-aerobic algal-bacterial photobioreactor configuration treating synthetic food waste digestate at different dilutions [27]. The process consisted of a two-stage anoxic-aerobic system engineered with biomass settling and recirculation without external CO_2 supplementation. Besides the open photobioreactor, the model was also applied to the enclosed anoxic reactor and the secondary settler, achieving a complete simulation of the continuous operation of the integrated system. A sensitivity analysis was applied to select the most relevant parameters of the model to estimate. Parameter estimation, which aims at fitting a given mathematical model to observed data, was conducted in the present work using a robust estimator to deal with the uncertainties imposed by some unreliable measurements. Parameter estimation in the settler was carried out to estimate the main parameters related to settleability properties, which are not well-established in microalgae-bacteria processes. The simulation results closely match the experimental data, further validating the accuracy of our model and its potential for further application in the system operation, control, and monitoring. The calibrated model could be used to evaluate the performance of the anoxic-aerobic configuration under different scenarios for municipal wastewater treatment, digestate treatment, or industrial wastewater treatment. Similarly, the model's reliability instills confidence in designing and applying model-based control strategies, such as Model Predictive Control (MPC), which can successfully handle the complex dynamics, interactions, and process constraints inherent to this system.

2. Materials and methods

2.1. Experimental plant description

Experimental data published in [27] from an anoxic-aerobic microalgal-bacterial photobioreactor configuration with biomass recycling treating synthetic food waste digestate (SFWD) was used to calibrate the model. The authors operated the anoxic-aerobic system at the Institute of Sustainable Processes of the University of Valladolid (Spain) from July to December 2019 [27]. The system (Fig. 1) comprised an open photobioreactor with a working volume of 9.15 L and was illuminated for 12 h daily by LED lamps (1314 ± 12 $\mu E/m^2s$). The anoxic reactor consisted of a gas-tight tank with a total working volume of 2.85 L maintained in the dark. The SFWD was fed to the anoxic tank at 1.2 L/d, continuously overflowing by gravity into the aerobic photobioreactor. The algal-bacterial broth was recycled at 2.4 L/d from the photobioreactor to the anoxic tank. An Imhoff cone with a volume of 1 L and interconnected to the outlet of the photobioreactor was used as a settler. The algal-bacterial biomass settled was recycled from the bottom of the settler into the anoxic tank at 0.6 L/d. Biomass was wasted from the bottom of the secondary settler to maintain the solids retention time (SRT) at 18 d. The system was operated continuously at a Hydraulic Retention Time (HRT) of 10 days and a temperature of 27 ± 2 °C. The experimental set-up was operated for 138 days under step changes in SFWD load: during the first stage (Stage I), the anoxic-aerobic system was fed with 25 % diluted SFWD, then SFWD load was increased to 50 % (Stage II), and finally increased to 100 % during the last stage of operation (Stage III). Further details of SFWD composition, experimental set-up, operational conditions, and results are provided in [27].

2.2. Experimental data

The model was calibrated and validated with data from 138 days of operation of the experimental plant [27]. The variables included in the model calibration were the results obtained for influent SFWD, anoxic tank, photobioreactor, settled biomass, and effluent in terms of concentration of dissolved oxygen (DO) concentration, pH, dissolved organic carbon (TOC), inorganic carbon (IC), dissolved N species (total nitrogen (TN), $N-NH_4^+$, $N-NO_2^-$, $N-NO_3^-$), dissolved phosphate ($P-PO_4^{3-}$), and biomass concentration, expressed as the total suspended solids (TSS) concentration. DO and pH were measured daily, whereas other variables were characterized twice a week.

To comprehensively capture in the model the dynamics of the anoxic-aerobic photobioreactor configuration treating different dilutions of digestate, data from various operational conditions were divided into two datasets, one devoted to parameter estimation in the reactors and the settler and the second one for model validation. Specifically, data from stage II and 25 days of stage III (50 % and 100 % digestate, respectively) were used for parameter estimation. Validation was then conducted using data from the first stage (25 % digestate – 40 days of operation) and days 116 to 138 from stage III (undiluted digestate – 22 days of operation).

2.3. Modeling

Similar to previous research in anoxic-aerobic systems [26,27], the model was built over the assumption that significant removals of $N-NH_4^+$, IC, and $P-PO_4^{3-}$, were mainly attributed to the contribution of the photobioreactor. In this work, eight key output variables were considered: TSS and TOC concentration in the photobioreactor and anoxic reactor; and dissolved oxygen, IC, $N-NH_4^+$ and $P-PO_4^{3-}$ in the photobioreactor. In the settler, TSS concentration in the effluent and the biomass wastage stream were considered output variables to adjust in the optimization problem.

As previously referred, biomass concentration in both reactors and settler was measured twice a week using standard procedures to determine the concentration of TSS and Volatile Suspended Solids (VSS). In the model used in this study, the concentrations of particulate components are expressed in terms of the Chemical Oxygen Demand (COD). Results from COD tests developed in [27] were used here to obtain the ratio VSS/COD used in the model. In the simulation, the average value of the experimental ratio gTSS/gCOD used was 1.28.

The microalgae-bacteria model was implemented in the dynamic simulation environment PROOSIS®.

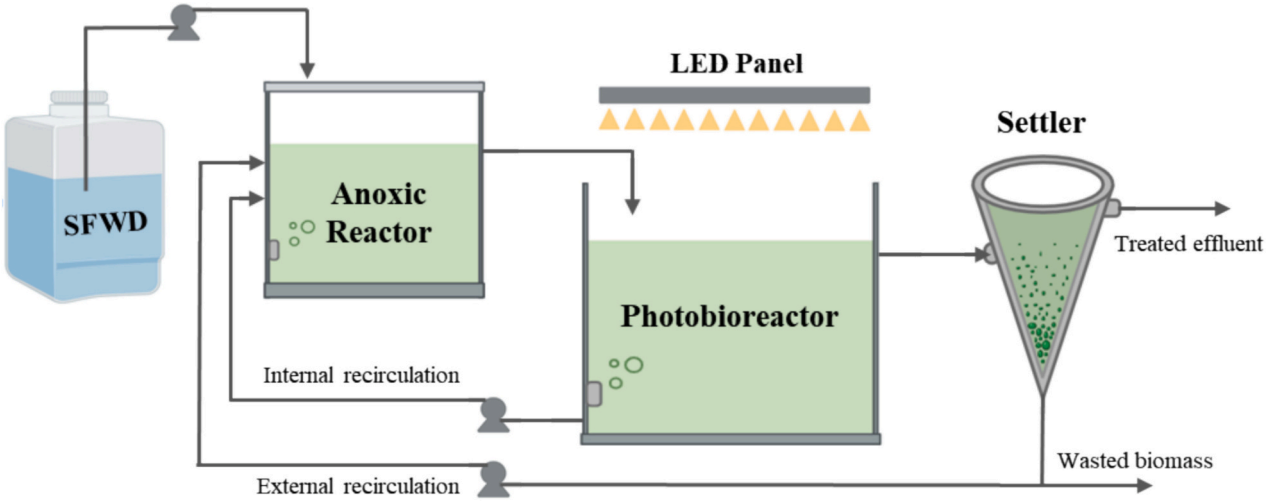

Fig. 1. Schematic of the anoxic-aerobic algal-bacterial photobioreactor configuration.

2.3.1. Photobioreactor and anoxic unit modeling

In the present work, the model BIO_ALGAE2 [20] (with some minor modifications) was used to represent the biochemical reactions and processes in both anoxic and aerobic reactors operating under the conditions described in [27]. The model BIO_ALGAE2 uses the standard nomenclature of the IWA models and considers 19 components −6 particulate and 13 dissolved– implicated as variables in the physical, chemical, and biokinetic processes. These components are described in [18], as well as their main role in the processes and their interactions with other components. The process rates of the model (Table S1.1), factors equations (Table S1.2), the matrix of stoichiometric parameters (Table S1.3), the values of parameters (Table S1.4), and fractions of carbon, hydrogen, oxygen, nitrogen in microalgae and bacteria biomass (Table S1.5), and a summary of the mathematical expressions of the stoichiometric coefficients (Table S1.6) are described in the Supplementary Material S1. Model modifications considered in the present work (Table S1.1) were related to the radiation factor (used in equations describing the microalgae growth (ρ_1 and ρ_2)) and the addition of one factor in the equation representing the aerobic growth of heterotrophic bacteria on dissolved nitrate (ρ_6) to indicate that when ammonium (or ammonia) and nitrate are both present, ammonium is generally preferred. Differences in a few stoichiometric parameters were also considered (Table S1.3).

Since this work aims to simulate the anoxic-aerobic configuration (and use that) to predict nutrient removal, it is helpful to emphasize the main reactions in each reactor. Table 1 summarizes the main reactions concerning microorganisms' activity in each reactor. Reactions related to chemical equilibrium were assumed to occur in the photobioreactor and anoxic reactor, while the transfer of gases was considered to occur only in the photobioreactor since the anoxic reactor corresponded to an enclosed unit. Evaporation was also considered in the mass balance expression in the photobioreactor.

2.3.2. Settler modeling

The settler was described using the mass-balance expressions of the model from Takács et al. [28]. The model is a multi-layer dynamic model for the clarification and thickening processes based on the solids flux concept and mass balance around each layer of a one-dimensional settler. This model can simulate the solids profile throughout the settling column, including the underflow and effluent suspended solids concentrations under steady-state and dynamic conditions. The model uses a particular settling velocity equation to simulate the settling velocity of dilute and more concentrated suspensions (Eq. S2.10 in Supplementary Material S2). The fundamental aspects and equations of the model (by Takács et al. [28]) are summarized in Supplementary

Table 1
Processes describing anoxic/aerobic reactions.

	Process	Anoxic Reactor	Aerobic Reactor
Microalgae processes	Growth on S_{NH4}	Not Considered	Considered
	Growth on S_{NO3}	Not Considered	Considered
	Endogenous respiration	Considered	Considered
	Decay	Considered	Considered
Heterotrophic bacteria processes	Aerobic growth on S_{NH4}	Not Considered	Considered
	Aerobic growth on S_{NO3}	Not Considered	Considered
	Anoxic growth on S_{NO2} (denitrification on S_{NO2})	Considered	Considered
	Anoxic growth on S_{NO3} (denitrification on S_{NO3})	Considered	Considered
	Aerobic endogenous respiration	Not Considered	Considered
	Anoxic endogenous respiration	Considered	Considered
	Decay	Considered	Considered
Autotrophic bacteria processes	Growth of X_{AOB}	Not Considered	Considered
	Growth of X_{NOB}	Not Considered	Considered
	Endogenous respiration of X_{AOB}	Considered	Considered
	Endogenous respiration of X_{NOB}	Considered	Considered
	Decay of X_{AOB}	Considered	Considered
	Decay of X_{NOB}	Considered	Considered
Hydrolysis	Hydrolysis	Considered	Considered
Chemical equilibrium	Chemical equilibrium $CO_2 \leftrightarrow HCO_3^-$	Considered	Considered
	Chemical equilibrium $HCO_3^- \leftrightarrow CO_3^{2-}$	Considered	Considered
	Chemical equilibrium $NH_4^+ \leftrightarrow NH_3$	Considered	Considered
	Chemical equilibrium $H^+ \leftrightarrow OH^-$	Considered	Considered
Transfer of gases	S_{O2} transfer to the atmosphere	Not Considered	Considered
	S_{CO2} transfer to the atmosphere	Not Considered	Considered
	S_{NH3} transfer to the atmosphere	Not Considered	Considered

Material S2.

This work considers a 10-layer settler of equal volume and assumes that no biological reactions occur in the settler. The model only considers biomass dynamics to predict the biomass concentration in each layer of the settler. Thus, in order to estimate the concentration of the components in the settler (and in the external recirculation and effluent), this assumption implies: (1) the concentration of dissolved components in the settler is assumed to be the same as in the photobioreactor, and (2) the percentage of each component of the biomass in the settler is assumed exactly equal that in the photobioreactor.

2.4. Sensitivity analysis

Previous to parameter estimation, a sensitivity analysis is needed to identify the parameters with the most significant impact on the model. The expression (1) describes the sensitivity functions from the *i*-output of the model concerning the *j*-parameter:

$$s_{i,j} = \frac{\partial y_i}{\partial p_j} \tag{1}$$

In order to compare the values of the sensitivities, scale factors (Eq. (2)) should be used to normalize them:

$$\bar{s}_{i,j} = \frac{p_j}{\bar{y}_i}\frac{\partial y_i}{\partial p_j} \tag{2}$$

Then, the norm of column *j* of the output sensitivity matrix (3)

$$\begin{bmatrix} s_{11} & s_{12} & \cdots & s_{1d} \\ s_{21} & s_{22} & \cdots & s_{2d} \\ \vdots & \vdots & \cdots & \vdots \\ s_{m1} & s_{m1} & \cdots & s_{md} \end{bmatrix} \tag{3}$$

provides a measure of the importance of parameter p_j in the value of the model outputs.

Given the dynamic model (4),

$$\dot{x}(t) = f(x(t), u(t), p)\ \mathrm{y}(t) = g(x(t), u(t), p) \tag{4}$$

The sensitivities can be obtained integrating in parallel the so-called extended model:

$$\frac{d}{dt}\frac{\partial x}{\partial p} = \frac{\partial f}{\partial x}\frac{\partial x}{\partial p} + \frac{\partial f}{\partial p} \tag{5}$$

$$\frac{\partial y}{\partial p} = \frac{\partial g}{\partial x}\frac{\partial x}{\partial p} + \frac{\partial g}{\partial p} \tag{6}$$

2.5. Parameter estimation

2.5.1. Sequential optimization

The numerical resolution approach used in the present work to solve the parameter estimation problem was the sequential approach (using simulation). The approach to solving a parameter estimation problem in terms of optimization considers that for each value of the vector of parameters $\boldsymbol{\theta}$ (decision variables), the model predicts the system's response $\hat{y}(t, \boldsymbol{\theta})$ in each experiment over time *t*. For this purpose, a set of data samples from the inputs $\boldsymbol{u}(t)$ and outputs $\boldsymbol{y}(t)$ of the process were selected as indicated above (Section 2.2). The exact sequence of process inputs $\boldsymbol{u}(t)$ applied to the process is also used in the model, and both outputs $\boldsymbol{y}(t)$ from the process and $\hat{\boldsymbol{y}}(t, \boldsymbol{\theta})$ from the simulation are compared at every sampling time *t*. For each *t*, the prediction error $\hat{\boldsymbol{y}}(t, \boldsymbol{\theta}) - \boldsymbol{y}(t)$ indicates model goodness, and the parameterization procedure looks for the set of model parameters $\boldsymbol{\theta}$ that minimizes the cost function of the prediction errors. The parameter estimation problem can be formulated as a dynamic optimization problem, which can be solved through nonlinear programming (NLP) software using a control vector parameterization technique and a proper procedure for computing the cost function, following the architecture of Fig. 2. This work uses the SNOPT algorithm, a well-known sequential quadratic programming (SQP) code for nonlinear optimization within the PROOSIS® dynamic simulation environment. The selected integration method was IDAS.

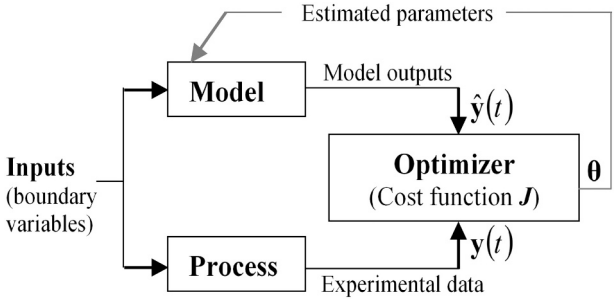

Fig. 2. Estimator in sequential optimization.

2.5.2. Robust estimation

Although there are several methods for obtaining the statistically coherent value of variables and estimating the parameters of the mathematical model based on available data, the weighted least squares (WLS) method is used most frequently. The estimator (Eq. (7)) consists of the squared difference between the measurement *y* and the model prediction $\hat{y}$. The differences are scaled with their respective standard deviation σ to account for varying dimensions of the model. This method assumes that measurement errors follow the Normal distribution model. The assumption of Normal distribution can be severely violated if one or more gross errors, which are not easy to detect, are present in the measured data set, even though most of the data conforms to a Normal distribution, resulting in poor or deviated estimates [29].

$$J_{LS} = \frac{1}{2}\left[((\hat{\boldsymbol{y}} - \boldsymbol{y})/\sigma)^2\right] \tag{7}$$

Thus, robust estimation can be understood as "insensitivity to large deviations from idealized hypotheses" for which the estimator is optimized [30]. To define the concept of robust estimation, let us consider a set of observations $\{y_1, \cdots, y_n\}$ drawn from some distribution $h(x)$; this set will be used to estimate some parameters θ let $\hat{\theta}_n$ to be the estimate. The sampling distribution of this estimate is noted as $\varphi(\hat{\theta}_n, h)$ and depends upon $h(x)$. However, $h(x)$ is not typically known, and only have a more or less valid model, say $f(x)$. Roughly speaking $\hat{\theta}_n$ is robust if it scarcely depends upon the difference between $h(x)$ and $f(x)$. i.e. we expect $\varphi(\hat{\theta}_n, h)$ and $\varphi(\hat{\theta}_n, f)$ to be close together.

More precisely, $\hat{\theta}_n$ is said to be robust with respect to distribution *f* (and to *h*) if

$$d(h,f) < \eta \Longrightarrow d[\varphi(\hat{\theta}_n, h), \varphi(\hat{\theta}_n, f)] < \epsilon \tag{8}$$

For small positive ϵ and η, and $d(h,f)$ defines the distance between the distributions *h* and *f*, associated with the measures of the plant and the outputs on the simulation model [31].

Robust statistics provides methods that emulate conventional statistical ones but are limited affected by spurious values or other deviations from the reference statistical distribution model. Among the robust estimators, M-estimators (the generalization of the Maximum Likelihood Estimator) have been successfully applied to several problems in the chemical process industry. The review presented in [29], which analyses 50 estimators (48 robust estimators), shows that the Contaminated Normal (quasi-robust), Welsch, Hampel, Fair, Lorentzian, Correntropy, and Cauchy M-estimators were the most used for regression analysis in chemical engineering problems.

The Fair function is a convex estimator with continuous first and second order derivatives. It is defined in (9), where $c \in \mathbb{R}+$ is a user-

defined fitting parameter to tune the slope for large residues.

$$J_{FF} = c^2 \left[\frac{\left|\frac{\hat{y}-y}{\sigma}\right|}{c} - ln\left(1 + \frac{\left|\frac{\hat{y}-y}{\sigma}\right|}{c}\right) \right] \tag{9}$$

M-estimators are robust because of their intrinsic mathematical structure, which renders the estimation less sensitive to spurious deviations [30–32]. These estimators, which use cost functions different from least squares (LS) or WLS, tend to value most of the data around the mean and ignore the influence of spurious values (usually located far from the mean) simultaneously. This performance is represented in Fig. 3, which compare the fair estimator (9) and the LS estimator (7), evidencing the influence of scaled error over the estimator function. Thus, an accurate regression can be performed using robust estimators even if nothing is known a priori about outliers or the structure of gross errors.

In the present work, the Fair function estimator was used as a robust objective function J for parameter estimation. The final dynamic optimization problem then reads:

$$\min_{\theta} J(\hat{\theta}, \theta) = \sum_{j \in M} c^2 \left[\frac{|\varepsilon_j|}{c} - ln\left(1 + \frac{|\varepsilon_j|}{c}\right) \right] \tag{10}$$

Subject to constraints imposed by the model (11) and upper and lower limits on the values of the parameters (12), states (13), and outputs (14),

$$\begin{aligned} \frac{d\boldsymbol{x}(t)}{dt} &= \boldsymbol{f}(\boldsymbol{x}(t), \boldsymbol{u}(t), \boldsymbol{\theta}, t) \\ \hat{\boldsymbol{y}}(t) &= \boldsymbol{g}(\boldsymbol{x}(t), \boldsymbol{u}(t), \boldsymbol{\theta}, t) \end{aligned} \tag{11}$$

$$\underline{\boldsymbol{\theta}} \le \hat{\boldsymbol{\theta}} \le \overline{\boldsymbol{\theta}} \tag{12}$$

$$\underline{\boldsymbol{x}} \le \hat{\boldsymbol{x}} \le \overline{\boldsymbol{x}} \tag{13}$$

$$\underline{\boldsymbol{y}} \le \hat{\boldsymbol{y}} \le \overline{\boldsymbol{y}} \tag{14}$$

where $\varepsilon_j = (\hat{\boldsymbol{y}}(t_j, \hat{\theta}) - \boldsymbol{y}(t_j))/\sigma_m$ is the error between available process measurements $\boldsymbol{y}(t_j)$ and their estimated values $\hat{\boldsymbol{y}}(t_j, \hat{\theta})$ limited between user-defined minimum and maximum values (Eqs. (12)–(14)). Besides robust properties, the simplicity of tuning (just one tuning parameter) is another remarkable advantage of the Fair estimator. In the present work, all simulations were carried out using a value of c = 2.9 in the tuning parameter of the cost function (Eq. (10)).

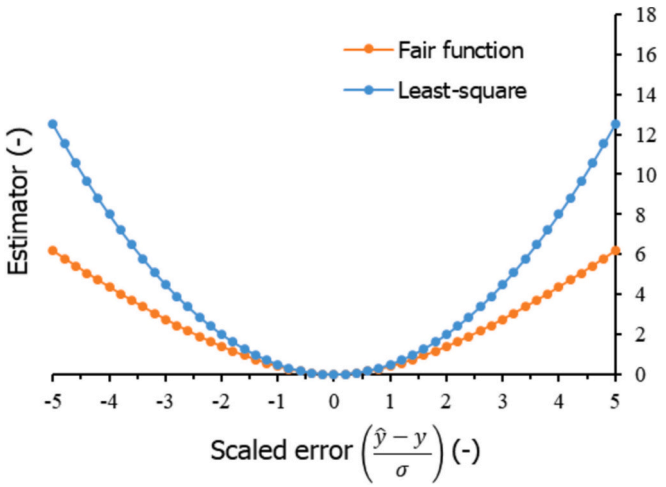

Fig. 3. Comparison of Least squares and Fair function (c = 3) estimators.

2.5.3. Considerations for robust parameter estimation in the anoxic-aerobic configuration

The initial concentration of the components in the reactors and the settler used to conduct the model simulation are shown in Tables S3.1 and S3.2, respectively, in Supplementary Material S3.

Table S4.1 (Supplementary Material S4) shows the limits for decision variables (Eq. (12)) and the initial values of parameters needed for parameter estimation via optimization in the anoxic and aerobic reactors; these values were established from a comprehensive review of similar studies reported in the literature [18,20,21,33]. For parameter estimation in the settler, the limits in the parameter related to the maximum settling velocity were selected according to values reported in the literature for microalgae systems or microalgae-bacteria consortia systems [34–36]. The ranges of the other parameters in the settling velocity equation were selected similar to those reported for activated sludge processes [28]. These values are shown in Table S4.2 in Supplementary Material S4. Then, the parameter estimation problem was solved for both reactors and the settler using the cost function (Eq. (10)) and SNOPT, a SQP optimization method for NLP problems connected to the model simulation.

In this study case, a robust objective function was relevant since gross errors may result from different sources:

- Many analytical procedures used to obtain the data are based on the use of external standards for calibration or data comparison. These solutions are subject to human errors during preparation
- Human errors in sample preparation and analysis can play a significant role in the accuracy of the experimental data obtained through analytical methods. For instance, errors in sample dilution preparation, non-homogeneous mixing, or sample degradation can lead to inaccurate results.
- The incorrect use of calibration curves: methods used to determine the concentration of dissolved NH_4^+, NO_2^-, NO_3^-, and PO_4^{3-} use calibration curves. The accuracy of the measurement largely depends on the expertise of the person analyzing the sample.
- The methods used to determine biomass concentration (TSS and VSS) can be significantly influenced by human errors in sample collection, such as non-homogeneous mixing of the sample and the presence of flocculated biomass. Additionally, procedure errors like filter obstruction, irregular oven and muffle temperatures, and violations of recommended drying times can also affect these measurements. Incorrect preservation of the samples (that can result in sample degradation and changes in the properties due to light and high-temperature exposition).
- The use of non-updated calibration curves in equipment.

Several decisions were made to improve the solution of parameter estimation, taking into account the specific experimental conditions:

1- Experimental data were obtained under illumination cycles of 12 h ON/12 h OFF [27] (considered in daily fraction with illumination between 2 am (0.083 d) and 2 pm (0.583 d)). Because of this, the time step used for the simulations was 0.1 d. Using superior time steps could result in an accuracy loss for the simulation of day/night cycles (and their influence over the model state variables).
2- The values of some variables vary significantly between day and night in the photobioreactor. Because samples were always drawn during illuminated periods, output data interpolation may result in non-representative data values of the internal dynamics in the photobioreactor. Therefore, only the recorded data at the exact time were considered in the cost function.
3- Since the values of experimental data broadly differ from stage I to stage III, different limits on state and output variables (Eqs. (13)–(14)) were considered in the optimization problem for each simulation stage.

2.6. Metrics for evaluate model performance

Two performance indexes were used to quantify the quality of the model adjustment to the experimental data: the mean absolute error (MAE) (Eq. (15)) and the mean absolute relative error (MARE) (Eq. (16)). Both criteria quantify the difference between model predictions and experimental data, and the MARE criteria normalize the error according to the magnitude of the measured variable. For both criteria, the closer the value to zero, the better the model performance. These values were computed for the complete experimental period (including the data set used for parameter estimation and model validation). The factor φ in the denominator of (16) is included to avoid division by zero in the case of experimental data $y_i = 0$.

$$MAE = \frac{1}{n}\cdot\sum_{i=1}^{n}|y_i - \hat{y}_i| \tag{15}$$

$$MARE = \frac{1}{n}\cdot\sum_{i=1}^{n}\frac{|y_i - \hat{y}_i|}{y_i + \varphi} \tag{16}$$

3. Results and discussion

3.1. Sensitivity analysis results

Sensitivity analyses were conducted for reactors and the settler using the software PROOSIS® with IDAS to compute the sensitivities in Eq. (2). Some model parameters are well-established in the literature, but others are strongly related to the operational conditions and microorganism strains used in the study. Thus, the sensitivity analysis was carried out considering a subset of all the model parameters to determine those significantly influencing the model outputs for this specific study case, providing crucial insights into the system's behavior.

The results of sensitivity analysis in both reactors indicated that model outputs are especially sensitive to the maximum specific growth rate of microalgae (μ_{ALG}) and heterotrophic bacteria (μ_H), the decay rate of microalgae ($k_{death,ALG}$) and heterotrophic bacteria ($k_{death,H}$), and the mass transfer coefficients for oxygen ($K_{la,\ O2}$), carbon dioxide ($K_{la,\ CO2}$), and ammonia ($K_{la,\ NH3}$). Graphical sensitivity analysis results for the previously referred parameters are presented in Figs. 4 and 5.

Fig. 4 A showcases the scaled sensitivity (Eq. (2)) for the dissolved ammonium (S_{NH_4}) in the photobioreactor. The graphical results highlight the significant sensitivity of the dissolved ammonium to the microalgae's maximum specific growth rate and the mass transfer coefficient for ammonia. These results show the high inverse effect of the maximum specific growth rate of microalgae over the dissolved ammonium: an increase in μ_{ALG} implies a decrease in S_{NH_4} in the photobioreactor due to the fact that microalgae are the primary consumers of dissolved ammonium. On the contrary, an increase in the microalgae decay rate mediates an increase in S_{NH_4}. In this facility, the mass transfer coefficient for ammonia significantly affects S_{NH_4} in the photobioreactor since ammonium is in equilibria with ammonia. Dissolved ammonium is also affected (to a lower extent) by the parameters relative to the activity of heterotrophic bacteria since they consume ammonium during aerobic growth.

Fig. 4 B shows the scaled sensitivity for the dissolved phosphate concentration (S_{PO_4}) in the photobioreactor. The results indicate that in this photobioreactor, the dissolved phosphate concentration is mainly affected by microalgae's maximum specific growth rate: an increase in μ_{ALG} promotes a significant reduction in the dissolved phosphate concentration. Because heterotrophic bacteria assimilate phosphate during growth, S_{PO_4} is also sensitive to the decay rate of these microorganisms. In less measure, dissolved phosphate concentration is affected by the microalgae decay rate and heterotrophic bacteria growth rate.

Fig. 4 C shows the results of the graphical sensitivity analysis over the IC in the photobioreactor. These results indicate that inorganic carbon is especially sensitive to the parameters concerning microalgae activity, especially to the maximum specific growth rate. Microalgae growth consumes inorganic carbon (in the forms of CO_2 and HCO_3), promoting a decrease in IC concentration, and microalgae death contributes to an increase in the dissolved IC in the photobioreactor. In addition, inorganic carbon is significantly affected by heterotrophic bacteria decay rate: an increase in $k_{death,H}$ promotes a decrease in the CO_2 release to the culture media product of heterotrophic bacteria respiration.

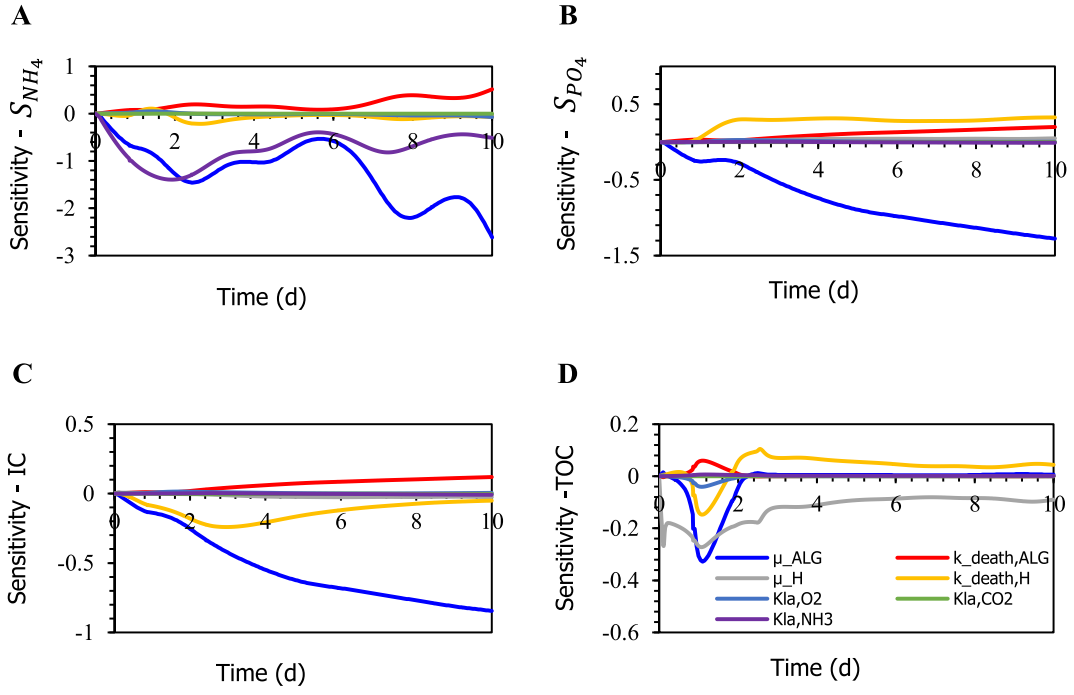

Fig. 4. Scaled sensitivities for the dissolved ammonium concentration (A), dissolved phosphate concentration (B), dissolved inorganic carbon concentration (C) and dissolved total organic carbon concentration (D) in the photobioreactor.

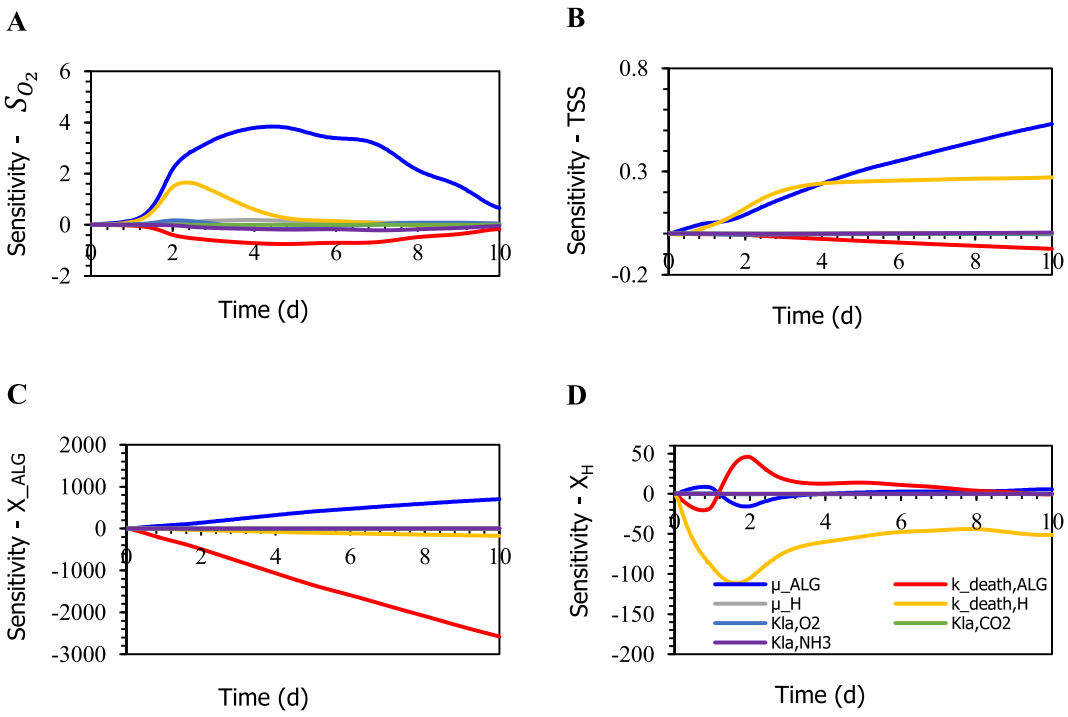

Fig. 5. Scaled sensitivity for the dissolved oxygen concentration (A) and for the total suspended solids concentration (B) in the photobioreactor. Unscaled sensitivity of microalgae biomass (C) and heterotrophic bacteria biomass concentration (D) in the photobioreactor.

Fig. 4 D represents the sensitivity results for the concentration of dissolved total organic carbon. The parameters related to heterotrophic bacteria growth and decay rates are the most influential over the TOC: an increase in the maximum specific growth rate of heterotrophic bacteria promotes a decrease in the dissolved TOC as result of significant assimilation of TOC into the heterotrophic biomass; on the contrary, an increase in the decay rate of heterotrophic bacteria implies a decrease in the assimilation of TOC by heterotrophic microorganisms (and, consequently, an increase in dissolved TOC in the photobioreactor).

With microalgae dominating the microbial population (50 % of the inoculum corresponded to microalgae biomass [27]), the maximum specific growth rate of microalgae was the parameter with the most substantial influence over the concentrations of NH_4^+, PO_4^{3-}, and IC in the photobioreactor, as confirmed in Fig. 4 A, B and C. Similarly, the maximum specific growth rate of heterotrophic bacteria was the most influential parameter over the dissolved TOC, as evidenced in Fig. 4 D. The differences in the values of graphical sensitivities observed during the period shown in Fig. 4 are the result of the stabilization of microbial populations in the photobioreactor.

The scaled sensitivity over the dissolved oxygen concentration (S_{O_2}) is represented in Fig. 5. It can be noted that the parameter with the most significant impact is the maximum specific growth rate of microalgae (because of photosynthesis, microalgae produce oxygen). The decay rate of microalgae is also influential in dissolved oxygen concentration. Heterotrophic bacteria consume oxygen for organic matter assimilation, explaining that parameters concerning heterotrophic bacteria activity are also influential over S_{O_2}. The mass transfer coefficient for oxygen is another parameter that impacts the dissolved oxygen concentration.

Fig. 5 B represents the scaled sensitivity of the total suspended solids concentration in the photobioreactor. Sensitivities of the parameters (without scaled, Eq. (1)) over microalgae concentration (X_{ALG}) and heterotrophic bacteria concentration (X_H) are presented in Fig. 5 C and D, respectively. Biomass concentration was considered equivalent to the sum of all particulate components in the model (microalgae biomass, bacteria biomass, inert particulate organic matter, and slowly biodegradable particulate organic matter). Biomass concentration is affected mainly by the maximum specific growth rate of microalgae. In addition, the inactivation growth rates of microalgae and heterotrophic bacteria influence the biomass concentration (due to the decrease in these populations and the formation of particulate organic matter from microalgae and bacteria decay). The effect of parameters represented over microalgae and heterotrophic bacteria biomass represented in Fig. 5 C and D evidences the critical role of normalization in sensitivity analysis for a correct interpretation of the results.

The model parameters of the settling velocity equation (Eq. S2.10 in Supplementary Material S2) in the model of Takács et al. [28] are usually obtained using nonlinear dynamic optimization. Fig. 6 represents the sensitivity analysis for these parameters over the TSS concentration in the effluent and wastage flow of the settler. Fig. 6 A confirms the influence over the biomass concentration in the effluent flow of the parameter related to the minimum attainable suspended solids concentration in the effluent (X_{min}), the parameter associated with the low concentration of solids (r_p), and the maximum theoretical settling velocity (V_0). Fig. 6 B represents the scaled sensitivity of TSS concentration in the wastage flow. This variable is affected by the maximum theoretical settling velocity and the settling parameters associated with the low solids concentration zone (r_p) and the hindered zone (r_h). Fig. 6 C and D represent the unscaled sensitivity for the biomass concentration in the effluent and wastage flow in the settler, respectively. Considerable scale differences between both analyzed output variables confirm the critical role of graphical and analytical sensitivity analysis (with and without normalization) as a previous stage in the calibration or parameter estimation process. This process ensures the precision and reliability of the results, enhancing the confidence in them.

The sensitivity analysis results in Figs. 4–6 provide valuable insights into the magnitude in which each selected parameter promotes a change in model outputs. These results underscore the importance of sensitivity analysis for each photobioreactor configuration, inoculum characteristics, and operational values.

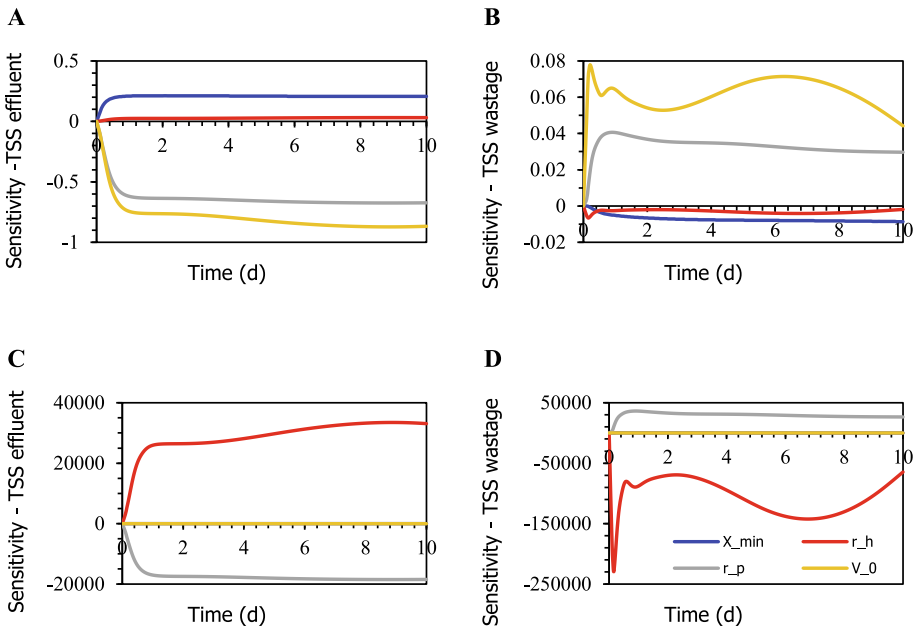

Fig. 6. Scaled sensitivity for the TSS concentration in the effluent (A) and in the wastage flow (B) in the settler. Unscaled sensitivity for biomass concentration in the effluent (C) and wastage flow (D).

3.2. *Parameter estimation in the anoxic-aerobic algal bacterial system*

Table 2 shows the values of the decision variables (parameters) for both reactors estimated in this study via optimization (Eq. (10)). All parameter values obtained are within the ranges reported in the literature for similar systems [18,20,21,33]. Parameter estimation was an essential aspect of this study since it provided the maximum specific growth and decay rates of the biomass, as well as information about parameters that strongly depended on photobioreactor size, shape, and stirring (like the mass transfer coefficients). The adequate calibration of these parameters provides insights into the system model that will be helpful in using the model for prediction and control purposes.

On the other hand, the settling properties of microalgae biomass (and consequently, the models to predict them) are nowadays an open-research field. Settling parameters in microalgae processes are widely dependent on the settler size, shape, and microorganism strains in the biomass. Therefore, those parameters should be determined for each specific configuration.

During the treatment of undiluted digestate, an increase in the TSS concentration in the effluent and a decrease in the average TSS concentration in the wastage stream were reported [27] as a consequence of a reduction of the settling efficiency (promoted by the decline in the biomass entering the settler from the photobioreactor). The research conducted in [27], when analyzing the microalgae populations, reported the dominance of *C. vulgaris*, *Tetradesmus obliquus*, and *Cryptomonas* sp. during stages I and II, while the dominant strains during stage III where *Chlorella vulgaris* and *Pseudanabaena* sp. Similarly, considerable differences in total microalgae densities per liter and per gram of VSS, as well as in the total microalgae biovolume during stage III, were reported [27]. Therefore, the high differences noted for the TSS concentration in the effluent and wastage flow during stage III were attributed to the reduction of the settling efficiency, differences in microalgae densities, and the different populations of microorganisms reported for this stage (consequently, these substantial changes in biomass characteristics imply different settling velocities and different values in the parameters related to biomass concentration). The previous assumption underscores the importance of estimating parameters in such a way that may be able to describe stages with remarkable differences in biomass composition. For this purpose, a sigmoid function (Fig. 7) was used to represent the variation of parameter values during the experiment. According to sigmoid function, each parameter $\widehat{\theta}_i = V_0, r_h, r_p$ varying between two values ($\widehat{\theta}_{i_{min}}$ and $K_i + \widehat{\theta}_{i_{min}}$). Then, instead of estimating the parameter values of settling velocity equation (V_0, r_h, r_p), the optimization problem estimates the parameter values of the sigmoid function in Eqs. (17) (19), where t represents the current simulation time, and t_c is the time instant where a significant change in biomass properties was considered. The parameter estimation was conducted, considering that a biomass composition change during the treatment of undiluted digestate (stage III). Data from stage II were used to determine the model parameters during the

Table 2
Values of estimated parameters in anoxic and aerobic reactor.

Parameter	Value [units]
μ_{ALG}	0.70 d^{-1}
μ_H	2.50 d^{-1}
$k_{death,ALG}$	0.05 d^{-1}
$k_{death,H}$	0.80 d^{-1}
$K_{la,\ O2}$	0.5 d^{-1}
$K_{la,\ CO2}$	2.17 d^{-1}
$K_{la,\ NH3}$	0.5 d^{-1}

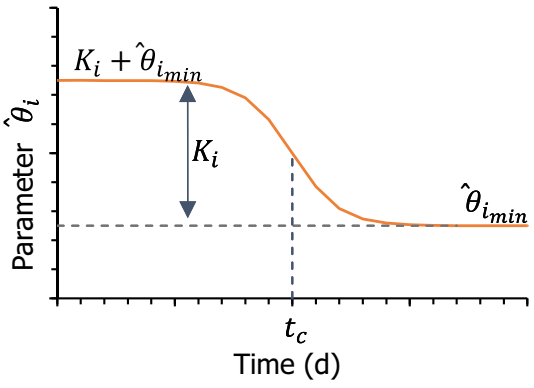

Fig. 7. Sigmoid function used to adjust the parameters of the settling velocity equation.

treatment of diluted digestate, while data from stage I were used for model validation using these parameter values. Data from stage III were used for parameter estimation (the first half of the data) and validation (the rest) during undiluted digestate treatment. The results of parameter estimation in the settler obtained via optimization in this study are shown in Table 3.

$$V_0 = K_{V_0} \cdot \frac{1}{1 + e^{(t - t_c)}} + V_{0min} \quad (17)$$

$$r_h = K_{r_h} \cdot \frac{1}{1 + e^{(t - t_c)}} + r_{hmin} \quad (18)$$

$$r_p = K_{r_p} \cdot \frac{1}{1 + e^{(t - t_c)}} + r_{pmin} \quad (19)$$

3.3. Model validation

Fig. 8 A, B, and C show simulation results and experimental measurements for S_{NH_4}, S_{PO_4}, and dissolved inorganic carbon in the photobioreactor, respectively. Ammonium and phosphate assimilation was mainly attributed to the biological processes occurring in the photobioreactor [27], which mediated high removal efficiencies of both nutrients during the treatment of diluted digestate, as confirmed during model validation. The model also reproduced the trend of increasing ammonium concentration and phosphate concentration observed in the photobioreactor during the treatment of undiluted digestate. The MARE values (Table 4 computed for ammonium concentration in the photobioreactor (below 0.72 for stages II and III), confirm the model's prediction capability. The model performance for phosphate, which was also quantified with the previously referred metrics, exhibits low MARE values for stages II and III (below 0.16 for both cases). High values of MARE during the first stage for ammonium and phosphate are caused by the normalization of this metric due to zero-close values reported experimentally for this stage. This error could be acceptable, taking into account that low values of MAE were obtained during this stage (and due to possible inaccuracies of the experimental methods for low concentrations of dissolved nutrients).

As reported in [27], high values of IC in the influent enhanced the activity of both microalgae and nitrifying bacteria. This intensive autotrophic activity demanded a high consumption of inorganic carbon in the photobioreactor, mainly during the first two operational stages (treating 25 % and 50 % diluted digestate, respectively). Thus, the model accurately reproduced the dynamic behavior of inorganic carbon concentration in the photobioreactor during the experiment. This was confirmed with the low values of MARE (Table 4 reported for all the period (below 0.23).

Results for parameter estimation and validation for the concentration of TOC in the anoxic reactor and the photobioreactor are presented in Fig. 9. The model reproduced the high removal efficiencies of TOC in both reactors, as reported in [27] for diluted digestate. The model also reproduced the decrease in TOC removal efficiency during the treatment of undiluted digestate. The MARE values (Table 4) during the three operational stages (values below 0.5 for both reactors) confirmed the model's capability to reproduce the total organic carbon concentration trend for both reactors.

The results in Figs. 8 and 9 showed that the model can predict nitrogen, phosphorous, and carbon removal efficiencies. In this study, the photobioreactor was operated under the specific operational conditions described in Section 2.1 and detailed in [27], corresponding with a constant HRT in the anoxic and aerobic reactor, and a constant SRT in the settler. Validation results (performed with data corresponding to dilutions of digestate different from those used in parameter estimation) confirm the model's prediction capability under different operational conditions. These validation results indicate that the calibrated model, with its broad applicability, could be used to simulate a wide range of operational conditions with minimum resources and time consumption. However, the real added value of the proper model calibration lies in applying the optimization approach to predict the optimal operation values (HRT, SRT, temperature, digestate dilutions…) that maximize the nutrient removal efficiency of this novel photobioreactor configuration.

Predicting dissolved oxygen is critical in fitting any biological model. In the photobioreactor, the dissolved oxygen concentration indicates the photosynthetic activity of microalgae and bacteria's heterotrophic and nitrifying activity. Fig. 10A presents the simulation results for the dissolved oxygen concentration in the photobioreactor and the recorded experimental data. Although dissolved oxygen was recorded once a day during the experiment; in the model simulation, daily variations in the dissolved oxygen concentration due to the effect of incident radiation are visible in Fig. 10B, which contain part of the data set used for model validation. As previously referred, the intense autotrophic activity during the treatment of 25 % diluted digestate supported high daily values of dissolved oxygen concentration during the illuminated periods in the first 40 days of experimentation. In addition, the high heterotrophic activity in the photobioreactor during the entire experiment mediated a decrease in dissolved oxygen values during dark periods for the three operational stages. During stages II and III, significant reductions in the maximum dissolved oxygen values during the illuminated periods were reported experimentally in [27] (and confirmed through the model simulation).

In this research, the model simulation results are paramount because of the lack of online measurements for fast-dynamic variables like dissolved oxygen. Model simulation provides invaluable insights into process behavior, enabling a comprehensive analysis of the dynamic behavior of various variables throughout the day, not just at the time of sample collection. As observed in the trend of simulated variables, the daily variations in dissolved oxygen concentration due to light/dark periods have practical implications for the daily trends of other variables in the photobioreactor. These changes during the day in the assimilation of ammonium, phosphates, inorganic carbon, and total organic carbon, as depicted in Figs. 8 and 9, respectively, provide valuable insights for the practical model application to operate and monitor the anoxic-aerobic configuration.

Concerning the dissolved oxygen results, during the first stage, low values of MARE were obtained (below 0.5), confirming the model's prediction capability. Instead, high values of MARE were reported for stages II and III, mainly due to high standard deviations reported for experimental data during stage II and to zero-close experimental values during stage III. Instead, low values of the MAE were reported during the complete period (Table 4). The quantitative analysis of this variable may be confusing because both the metrics used were calculated considering the average of all the data for the period. In this case, experimental data may vary significantly depending on the hour of the day, affecting the average value.

Table 3
Values of estimated parameters in the settler.

Parameter	Description	Value [units]
X_{min}	Minimum attainable suspended solids concentration in the effluent	50 mg/L
V_0	Maximum theoretical settling velocity (Eq. (17))	$K_{V_0} = 5.040$ dm/d $V_{0min} = 2.097$ dm/d
r_h	Settling parameter associated with the hindered settling component of settling velocity equation (Eq. (18))	$K_{r_h} = 4.33 \cdot 10^{-05}$ L/mg $r_{hmin} = 7.893 \cdot 10^{-10}$ L/mg
r_p	Settling parameter associated with the low concentration and slowly settling component of the suspension (Eq. (19))	$K_{r_p} = 2.933 \cdot 10^{-04}$ L/mg $r_{pmin} = 8.713 \cdot 10^{-04}$ L/mg
t_c	The time when a significant change in the biomass properties occurred (Eqs. (17)–(19))	88.9 d

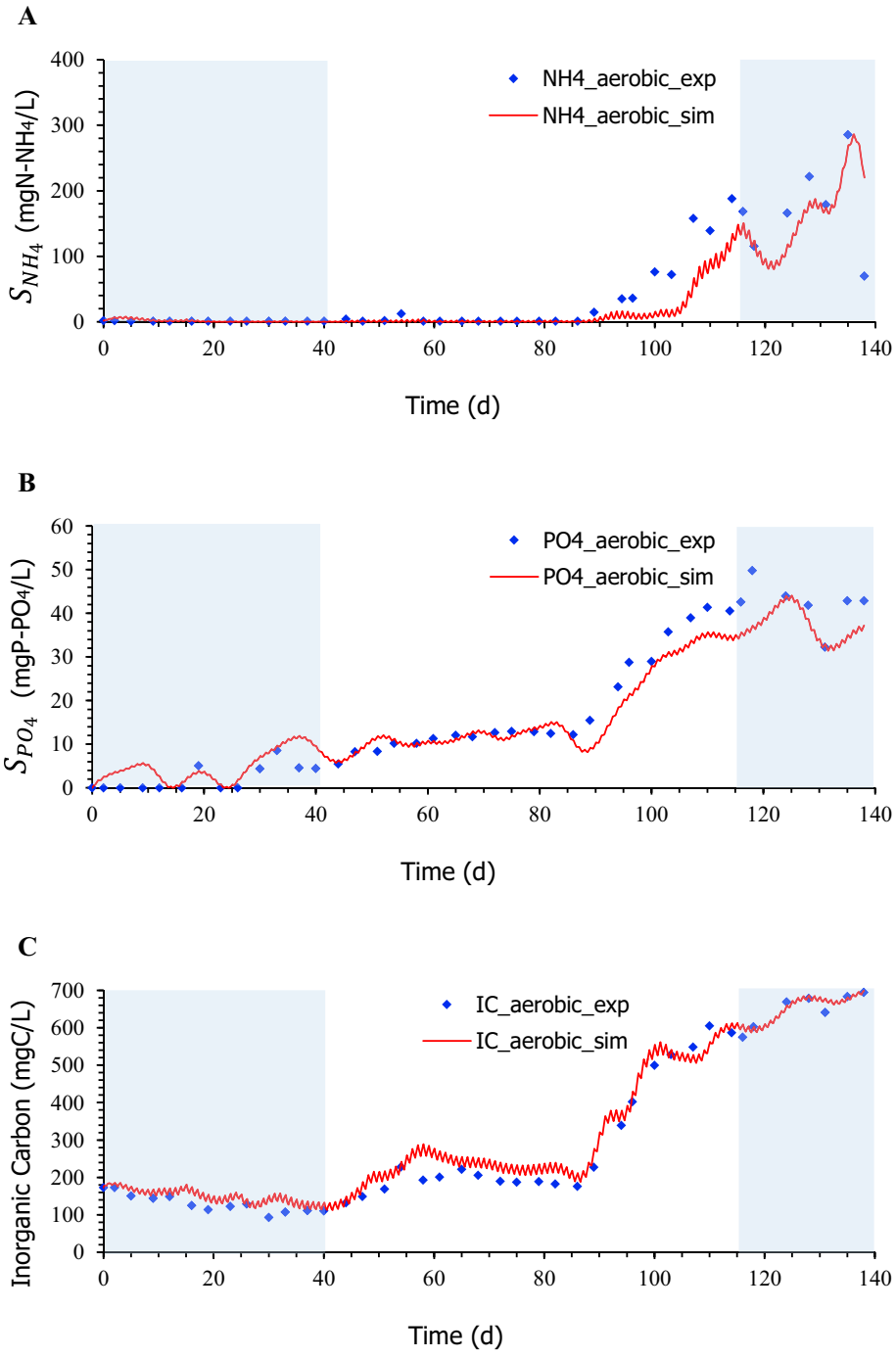

Fig. 8. Time course of the concentrations of dissolved ammonium (A), dissolved phosphate (B), and dissolved inorganic carbon (C) in the photobioreactor. White areas indicate the data sets used for parameter estimation, and blue shadow areas contain the data set used for model validation. (For interpretation of the references to color in this figure legend, the reader is referred to the web version of this article.)

Fig. 11 represents the biomass concentration in both reactors and the settler. Fig. 11 A and B show simulation results and experimental measurements for the concentration of TSS in the anoxic reactor and in the photobioreactor, respectively. The model reproduced the trend of the decrease in TSS concentration reported during stage III in both reactors [27]. Overall, the model proved effective in reproducing the dynamic behavior of biomass concentration. Small changes in the TSS concentration in the photobioreactor due to the daily variations in the light irradiation were observed, fundamentally due to the microalgae activity as the dominant group of the consortia. Thus, microalgae growth during the day increased the TSS concentration, and microalgae death at night decreased the TSS concentration. Low values of the MARE (below 0.35) were reported for both reactors during the experimental time (Table 4), which confirms the model prediction capability to reproduce the biomass dynamics.

Fig. 11 C represents the total suspended solids concentration in the effluent and biomass wastage stream, respectively. An increase in the TSS concentration in the effluent was reported during the treatment of undiluted digestate, likely due to the decrease in the settling efficiency, different dominant populations of microalgae, and differences in microalgae densities (as referred to by the authors of [27]), which presumably affects the sedimentation capability of the biomass. The

Table 4
Model evaluation for the three stages of experimentation.

	Stage I	Stage II	Stage III
Mean absolute error			
S_NH_4 - Photobioreactor	1.3877	1.5671	44.3109
S_PO_4 - Photobioreactor	2.7609	1.1039	5.3482
IC - Photobioreactor	26.6770	42.2906	23.1514
TOC - Anoxic Reactor	8.7098	21.6805	76.3308
TOC - Photobioreactor	9.3972	17.6676	39.2998
S_O_2 - Photobioreactor	3.4216	1.1678	0.3025
TSS - Anoxic Reactor	383.2931	348.3835	181.2617
TSS - Photobioreactor	167.9968	393.1145	196.3628
TSS - Effluent	20.9246	58.0595	108.3349
TSS - Wastage	1153.0377	1779.9657	2370.5445
Mean absolute relative error			
S_NH_4 - Photobioreactor	1.2013	0.7172	0.5138
S_PO_4 - Photobioreactor	14.5448	0.1055	0.1560
IC - Photobioreactor	0.2270	0.2274	0.0514
TOC - Anoxic Reactor	0.2641	0.4943	0.3594
TOC - Photobioreactor	0.3459	0.4781	0.3524
S_O_2 - Photobioreactor	0.4867	0.9884	2.1065
TSS - Anoxic Reactor	0.3145	0.3454	0.1598
TSS - Photobioreactor	0.1304	0.2625	0.0847
TSS - Effluent	0.2798	0.5922	0.4039
TSS - Wastage	0.1943	0.2138	1.2124

model reproduces the trend of increasing TSS concentration in the effluent during stage III. The low MARE values reported for the effluent biomass concentration confirm the match between experimental and simulated data (Table 4).

In the wastage flow, low values of the MARE (below 0.22) were reported during the treatment of undiluted digestate (Table 4), which confirms the model prediction capability. The high standard deviation reported for the experimental data during stage III in the wastage flow (4742 ± 2529) suggests the presence of flocculated biomass, which could be a source of gross error during the analytical procedure to quantify the biomass concentration. High experimental data dispersion in the TSS concentration in the waste flow makes it difficult for the model to fit during the treatment of undiluted digestate.

The model validation results (Figs. 8–11) have allowed the evaluation of the model's qualitative responses to input changes and the confirmation of its validity over long periods under changing conditions. Table 4 summarizes the computed criteria for the measured variables in each operational stage. Results for the MARE criteria (close to zero in most cases) confirm the model's capability to reproduce the experimental data. The MARE criteria generally constitute a reliable indicator of the model's goodness. However, the MARE value increases for small values of measured variables.

Simulation results revealed the model's versatility in photobioreactors with one or two stages, including sedimentation and biomass recirculation. The model's proficiency in replicating both rapid and slow

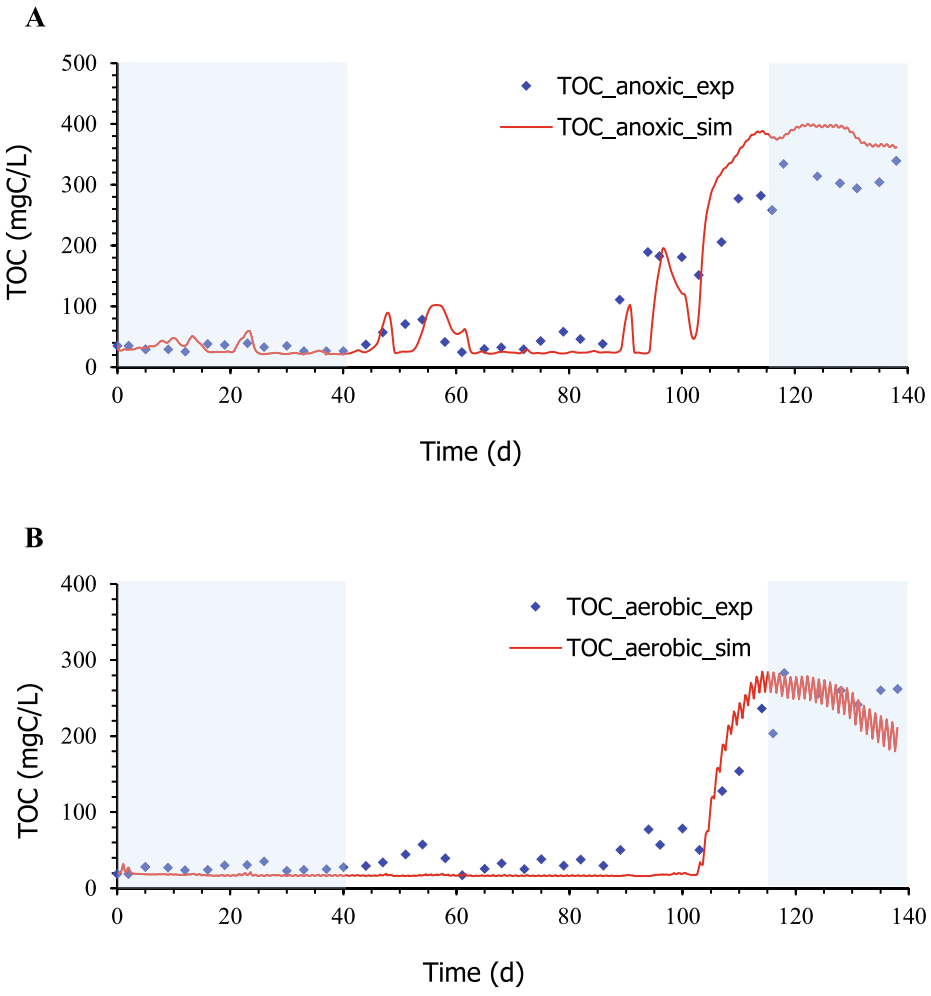

Fig. 9. Time course of the total organic carbon concentration in anoxic reactor (A) and in the photobioreactor (B). White areas indicate the data sets used for parameter estimation, and blue shadow areas contain the data set used for model validation. (For interpretation of the references to color in this figure legend, the reader is referred to the web version of this article.)

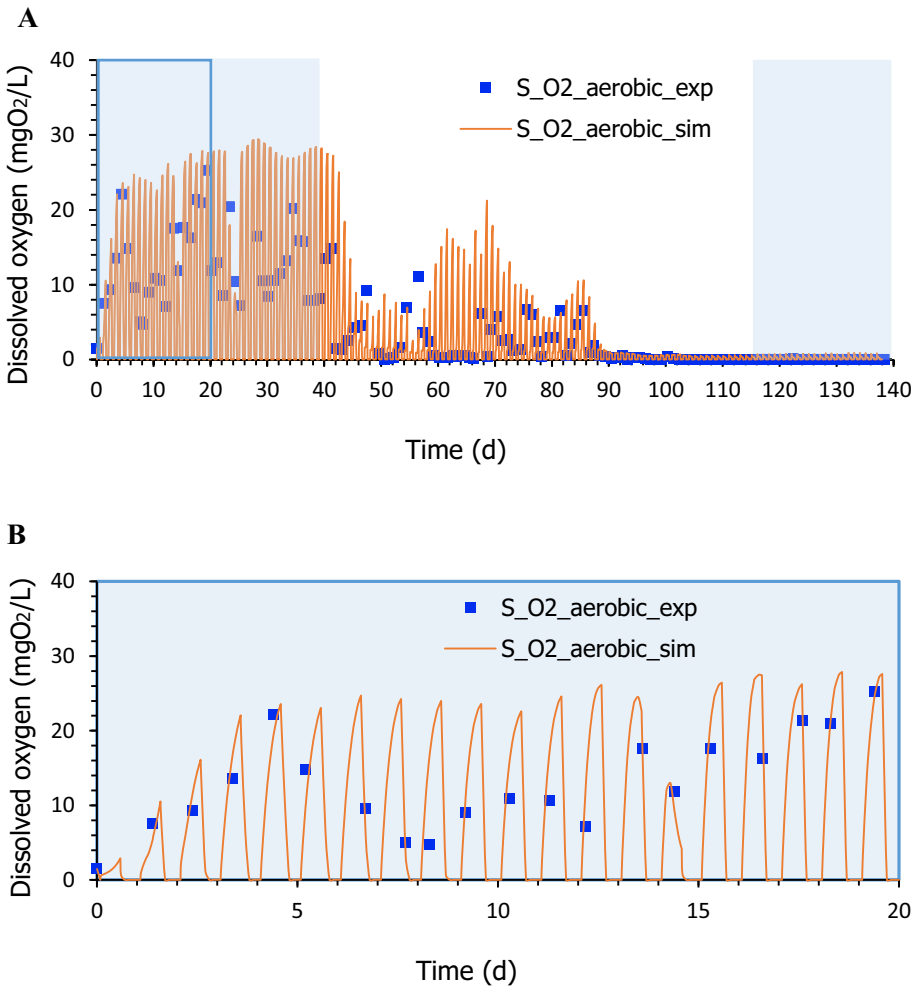

Fig. 10. Time course of the dissolved oxygen concentration in the photobioreactor during the experiment (A) (white areas contain the data sets used for parameter estimation, and blue shadow areas indicate the data set used for model validation). The blue rectangle delimited area shows the time course of the dissolved oxygen concentration during 20 days of data used for model validation (B). (For interpretation of the references to color in this figure legend, the reader is referred to the web version of this article.)

dynamics further reinforces its potential application to various biological processes, such as biogas upgrading processes with microalgae and the simultaneous treatment of digestates.

Aside from determining optimal operational conditions, the calibrated model is a valuable tool for systematically monitoring and controlling this process. Future implementation in the anoxic-aerobic configuration of state feedback control laws or model-based control techniques, such as MPC (successfully applied in other microalgae processes), can significantly enhance plant depuration efficiency and biomass yield. These control strategies' successful design and operation require information on all the system's states. However, many process variables cannot be directly measured online in this process. To face this drawback, the calibrated model, coupled with low investment in conventional sensors, would facilitate the design of a state estimator. This state estimator could provide corrected values online for all measured and unmeasured variables involved in the process, significantly reducing the time, human resources, and reagents needed in the analytical process monitoring, thereby enhancing cost-effectiveness and efficiency.

4. Conclusions

This paper presented the modeling and dynamic simulation of an anoxic-aerobic algal-bacterial photobioreactor for digestate treatment for the first time. Simulation results for the output variables considered in the anoxic-aerobic algal-bacteria photobioreactor configuration showed the model's capability to reproduce many system dynamic behavior features. However, some discrepancies were observed during the simulation of biomass concentration in the effluent and wastage flow in the settler. The model capability for prediction can be used to simulate the system's global behavior operating under several operational conditions while treating domestic or high-strength wastewaters. However, further research on modeling processes occurring under anoxic conditions should be conducted to improve the model's accuracy.

CRediT authorship contribution statement

Irina Bausa-Ortiz: Writing – review & editing, Writing – original draft, Visualization, Software, Methodology, Investigation. **Raúl Muñoz:** Writing – review & editing, Writing – original draft, Visualization, Supervision, Resources, Funding acquisition, Conceptualization. **Andrés F. Torres-Franco:** Writing – review & editing, Investigation, Formal analysis. **Smaranda P. Cristea:** Writing – review & editing, Supervision, Methodology. **Cesar de Prada:** Writing – review & editing, Writing – original draft, Visualization, Supervision, Software, Resources, Methodology, Funding acquisition, Conceptualization.

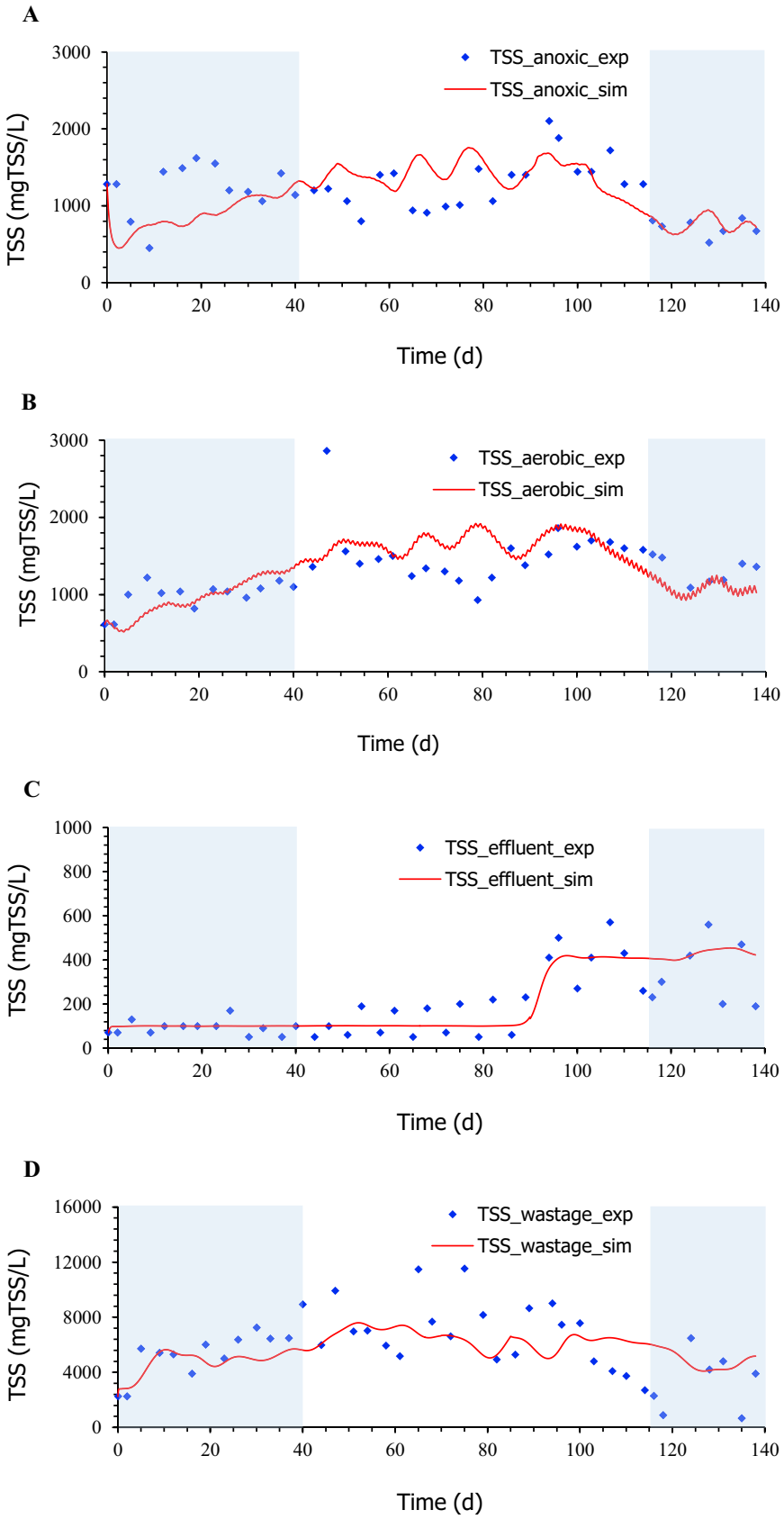

Fig. 11. Time course of the total suspended solids concentration in anoxic reactor (A) and in the photobioreactor (B). TSS concentration in the effluent (C) and wastage flow (D) of the settler. White areas indicate the data sets used for parameter estimation, and blue shadow areas contain the data set used for model validation. (For interpretation of the references to color in this figure legend, the reader is referred to the web version of this article.)

Declaration of competing interest

The authors declare that they have no known competing financial interests or personal relationships that could have appeared to influence the work reported in this paper.

Acknowledgments

This research was supported by Regional Government of Castilla y León and EU-FEDER program (CL-EI-2021-07, UIC 233, UIC 379), by Regional Government of Castilla y León and the European Social Fund (Order EDU/601/2020), and by the Project a-CIDiT (PID2021-123654OB-C31).

Appendix A. Supplementary data

Supplementary data to this article can be found online at https://doi.org/10.1016/j.algal.2025.103917.

Data availability

Data will be made available on request.

References

[1] K.J. Chae, J. Kang, Estimating the energy independence of a municipal wastewater treatment plant incorporating green energy resources, Energy Convers. Manag. 75 (2013) 664–672, https://doi.org/10.1016/j.enconman.2013.08.028.
[2] R. Muñoz, B. Guieysse, Algal-bacterial processes for the treatment of hazardous contaminants: a review, Water Res. 40 (15) (2006) 2799–2815, https://doi.org/10.1016/j.watres.2006.06.011.
[3] W.A.V. Stiles, et al., Using microalgae in the circular economy to valorise anaerobic digestate: challenges and opportunities, Bioresour. Technol. 267 (July) (2018) 732–742, https://doi.org/10.1016/j.biortech.2018.07.100.
[4] M. Ras, J.P. Steyer, O. Bernard, Temperature effect on microalgae: a crucial factor for outdoor production, Rev. Environ. Sci. Biotechnol. 12 (2) (2013) 153–164, https://doi.org/10.1007/s11157-013-9310-6.
[5] S.P. Singh, P. Singh, Effect of temperature and light on the growth of algae species: a review, Renew. Sust. Energ. Rev. 50 (2015) 431–444, https://doi.org/10.1016/j.rser.2015.05.024.
[6] V. Singh, V. Mishra, Evaluation of the effects of input variables on the growth of two microalgae classes during wastewater treatment, Water Res. 213 (February) (2022) 118165, https://doi.org/10.1016/j.watres.2022.118165.
[7] I. de Godos, et al., A comparative evaluation of microalgae for the degradation of piggery wastewater under photosynthetic oxygenation, Bioresour. Technol. 101 (14) (2010) 5150–5158, https://doi.org/10.1016/j.biortech.2010.02.010.
[8] Z. Arbib, J. Ruiz, P. Álvarez-Díaz, C. Garrido-Pérez, J.A. Perales, Capability of different microalgae species for phytoremediation processes: wastewater tertiary treatment, CO2 bio-fixation and low cost biofuels production, Water Res. 49 (2014) 465–474, https://doi.org/10.1016/j.watres.2013.10.036.
[9] E. Posadas, M. del M. Morales, C. Gomez, F.G. Acién, R. Muñoz, Influence of pH and CO2 source on the performance of microalgae-based secondary domestic wastewater treatment in outdoors pilot raceways, Chem. Eng. J. 265 (2015) 239–248, https://doi.org/10.1016/j.cej.2014.12.059.
[10] J. García, R. Mujeriego, M. Hernández-Mariné, High rate algal pond operating strategies for urban wastewater nitrogen removal, J. Appl. Phycol. 12 (3–5) (2000) 331–339, https://doi.org/10.1023/a:1008146421368.
[11] A. Torres-Franco, F. Passos, C. Figueredo, C. Mota, R. Muñoz, Current advances in microalgae-based treatment of high-strength wastewaters: challenges and opportunities to enhance wastewater treatment performance, Rev. Environ. Sci. Biotechnol. 20 (1) (2021) 209–235, https://doi.org/10.1007/s11157-020-09556-8.
[12] Y.K. Leong, C.Y. Huang, J.S. Chang, Pollution prevention and waste phycoremediation by algal-based wastewater treatment technologies: the applications of high-rate algal ponds (HRAPs) and algal turf scrubber (ATS), J. Environ. Manag. 296 (June) (2021), https://doi.org/10.1016/j.jenvman.2021.113193.
[13] D.L. Sutherland, J. Park, P.J. Ralph, R.J. Craggs, Improved microalgal productivity and nutrient removal through operating wastewater high rate algal ponds in series, Algal Res. 47 (March) (2020) 101850, https://doi.org/10.1016/j.algal.2020.101850.
[14] D.L. Sutherland, J. Park, S. Heubeck, P.J. Ralph, R.J. Craggs, Size matters – microalgae production and nutrient removal in wastewater treatment high rate algal ponds of three different sizes, Algal Res. 45 (July 2019) (2020) 101734, https://doi.org/10.1016/j.algal.2019.101734.
[15] I.B. Magalhães, et al., Advancements in high-rate algal pond technology for enhanced wastewater treatment and biomass production: a review, J. Water Process Eng. 66 (July) (2024), https://doi.org/10.1016/j.jwpe.2024.105929.
[16] M. Henze, W. Gujer, T. Mino, M. van Loosdrecht, Activated Sludge Models ASM1, ASM2, ASM2d and ASM3, IWA Publishing, 2000.
[17] P. Reichert, et al., River Water Quality Model No. 1 (RWQM1): II. Biochemical Process Equations, APA, 2001.
[18] A. Solimeno, L. Parker, T. Lundquist, J. García, Integral microalgae-bacteria model (BIO_ALGAE): application to wastewater high rate algal ponds, Sci. Total Environ. 601–602 (Dec. 2017) 646–657, https://doi.org/10.1016/j.scitotenv.2017.05.215.
[19] A. Solimeno, J. García, Microalgae and bacteria dynamics in high rate algal ponds based on modelling results: long-term application of BIO_ALGAE model, Sci. Total Environ. 650 (Feb. 2019) 1818–1831, https://doi.org/10.1016/j.scitotenv.2018.09.345.
[20] A. Solimeno, C. Gómez-Serrano, F.G. Acién, BIO_ALGAE 2: improved model of microalgae and bacteria consortia for wastewater treatment, Environ. Sci. Pollut. Res. 26 (25) (2019) 25855–25868, https://doi.org/10.1007/s11356-019-05824-5.
[21] F. Casagli, G. Zuccaro, O. Bernard, J.P. Steyer, E. Ficara, ALBA: a comprehensive growth model to optimize algae-bacteria wastewater treatment in raceway ponds, Water Res. 190 (Feb. 2021), https://doi.org/10.1016/j.watres.2020.116734.
[22] A. Sánchez-Zurano, E. Rodríguez-Miranda, J.L. Guzmán, F.G. Acién-Fernández, J. M. Fernández-sevilla, E.M. Grima, ABACO: a new model of microalgae-bacteria consortia for biological treatment of wastewaters, Appl. Sci. 11 (3) (Feb. 2021) 1–24, https://doi.org/10.3390/app11030998.
[23] I. de Godos, et al., Assessing carbon and nitrogen removal in a novel anoxic-aerobic cyanobacterial-bacterial photobioreactor configuration with enhanced biomass sedimentation, Water Res. 61 (2014) 77–85, https://doi.org/10.1016/j.watres.2014.04.050.
[24] Z. Dhaouefi, et al., Assessing textile wastewater treatment in an anoxic-aerobic photobioreactor and the potential of the treated water for irrigation, Algal Res. 29 (August 2017) (2018) 170–178, https://doi.org/10.1016/j.algal.2017.11.032.
[25] D. García, C. Alcántara, S. Blanco, R. Pérez, S. Bolado, R. Muñoz, Enhanced carbon, nitrogen and phosphorus removal from domestic wastewater in a novel anoxic-aerobic photobioreactor coupled with biogas upgrading, Chem. Eng. J. 313 (2017) 424–434, https://doi.org/10.1016/j.cej.2016.12.054.
[26] C. Alcántara, et al., Evaluation of wastewater treatment in a novel anoxic-aerobic algal-bacterial photobioreactor with biomass recycling through carbon and nitrogen mass balances, Bioresour. Technol. 191 (2015) 173–186, https://doi.org/10.1016/j.biortech.2015.04.125.
[27] A.F. Torres-Franco, et al., Assessment of the performance of an anoxic-aerobic microalgal-bacterial system treating digestate, Chemosphere 270 (2021), https://doi.org/10.1016/j.chemosphere.2020.129437.
[28] I. Takács, G.G. Patryioand, D. Nolasco, A dynamic model of the clarification-thickening process, Water Res. 25 (10) (1991) 1263–1271.
[29] D.Q.F. de Menezes, D.M. Prata, A.R. Secchi, J.C. Pinto, A review on robust M-estimators for regression analysis, Comput. Chem. Eng. 147 (2021), https://doi.org/10.1016/j.compchemeng.2021.107254.
[30] P.J. Huber, E.M. Ronchetti, Robust Statistics, Second Edi, John Wiley & Sons, New Jersey, 2009.
[31] W.J.J. Rey, Introduction to Robust and Quasi-robust Statistical Methods, Springer-Verlag, 1983, https://doi.org/10.1007/978-3-642-69389-2.
[32] P.J. Huber, Robust statistics, in: M. Lovric (Ed.), International Encyclopedia of Statistical Science, Springer, 2011, pp. 1248–1251, https://doi.org/10.1007/978-3-642-04898-2, ch. Robust Sta.
[33] I. Bausa, R. Muñoz, S. Podar, C. de Prada, Modeling and simulation of anoxic-aerobic algalbacterial photobioreactor for nutrients removal, in: L. Montastruc, S. Negny (Eds.), Computer-aided Chemical Engineering, 51 - Proceedings of the 32nd European Symposium on Computer Aided Process Engineering (ESCAPE32), June 12–15, 2022, Toulouse, France vol. 2, © 2022 Elsevier B.V. All rights reserved, 2022, pp. 151–156, https://doi.org/10.1016/B978-0-323-95879-0.50026-6, ch. Modeling a.
[34] S.K. Parakh, P. Praveen, K.C. Loh, Y.W. Tong, Integrating gravity settler with an algal membrane photobioreactor for in situ biomass concentration and harvesting, Bioresour. Technol. 315 (July) (2020), https://doi.org/10.1016/j.biortech.2020.123822.
[35] B.T. Smith, R.H. Davis, Particle concentration using inclined sedimentation via sludge accumulation and removal for algae harvesting, Chem. Eng. Sci. 91 (2013) 79–85, https://doi.org/10.1016/j.ces.2013.01.007.
[36] F. Passos, R. Gutiérrez, E. Uggetti, M. Garfí, J. García, I. Ferrer, Towards energy neutral microalgae-based wastewater treatment plants, Algal Res. 28 (May) (2017) 235–243, https://doi.org/10.1016/j.algal.2017.11.006.